Research on the Transport Mechanism of Tunnel Dust Based on FLUENT

Yuzhu Zhou, Dingyi Wei, Xin Lv, Zongzhi Wu, Zhiyong Shen, Chen Yu, Yang Mu, Tiantian Li

Abstract—**The increasing mechanization level that has emerged with the rapid development of tunnel construction has led to a growing problem of excessive dust concentration in tunnels. If not effectively managed, it can severely harm the health of workers and pose others safety hazards due to reduced visibility. Therefore, in this paper, a scaled model of a specific construction tunnel in Sichuan was established using Fluent to investigate the airflow distribution and dust transport mechanism inside the tunnel. Our results indicate that under on-site construction conditions, it takes 1800s for the dust concentration in the tunnel to reach the permissible level. When the velocity of the duct outlet was 16m/s and located 40m away from the workface, it took 1700s for the dust concentration to reach the permissible level. However, the optimal dust removal efficiency was achieved when the velocity of the duct outlet was 16m/s and the duct exit was 30m away from the workface, which resulted in a reduction to permissible levels in only 1300s of ventilation.**

Index Terms—**Construction tunnel, Dust concentration; Transport mechanism, Numerical simulation**

I. Introduction

Tunnel construction plays an important role in the process of infrastructure development [1,2], but a large amount of dust is generated during various stages of tunnel blasting. Not only are rocks shattered into dust under the pressure of the explosions but the shockwaves cause previously attached dust in the tunnel to become airborne again. Moreover, dust generated during blasting construction accounts for approximately 80% to 90% of the total dust. This dust can remain suspended in the air for extended periods, posing significant health risks to workers.

In addition to impacting the health of workers, dust also affects production and construction [3-5]. Suspended dust particles in the construction environment reduce visibility, obstructing the vision of workers and decreasing work efficiency. Furthermore, precision instruments may experience decreased accuracy due to dust, affecting the quality of construction. High concentrations of dust can also increase the risk of dust explosions. Many experts have conducted relevant research on the variations in dust during tunnel blasting to address these issues.

In the 1940s, Skochinsky et al.[6] conducted extensive experimental studies on the relationship between wind velocity and dust and identified the main factors that influence dust movement. Kyle[7] analyzed the relationship between dust concentration and airflow rate through on-site measurements at the workface and ultimately proposed the optimal dust removal airflow rate. Similarly, Irgibayev[8] conducted dispersion experiments on dust particles in ventilation tunnels and obtained distribution curves of dust concentration under different wind directions, then established a dust free settling model. Likewise, Feroze et al.[9] studied the concentration distribution and transport mechanisms of dust in enclosed spaces, and developed a CFD model for predicting the capture and emission of existing hoods for smoke extraction. Their model predicted that significantly increasing ventilation flow rates would have minimal improvement in smoke capture. Chung[10-12] proposed a model and concluded that particles and fluid eventually reach a state of relative equilibrium in motion.

Other authors have also employed numerical simulations to simulate the distribution and transport mechanism of dust concentrations at the workface[13]. Mikhail et al.[14] conducted dust diffusion experiments in tunnels to understand the influence of airflow distribution on dust dispersion, and they also analyzed the settling trajectories of dust particles. Koshiro et al.[15-17] simulated the transport of dust in fully mechanized workfaces and developed curtain dust removal technology based on field measurements. Cai et al.[18,19] utilized Fluent to simulate dust movement generated by belt transportation in tunnels and compared the results to field-measured dust concentrations. Additionally, Reed et al.[20] investigated the impact of ventilation methods in tunnels on dust transport through numerical simulation and optimized dust removal schemes based on on-site conditions. Hasheminasab[21] divided the airflow structure of advancing workfaces using the forced ventilation method into three zones and proposed a calculation model for dust

Manuscript received March 18, 2024; revised October 21, 2024.

This work was supported by the Doctoral Fund Project of Henan University of Engineering (Grant No.: D2022021); Key Research Projects Programme of Henan Higher Education Institutions (Grant No.: 23B440005).

Yuzhu Zhou is a Ph.D student at the School of Civil and Resources Engineering, University of Science and Technology Beijing, Beijing 100083, China. (e-mail: yx80612621@126.com).

Dingyi Wei is a lecturer at the School of Resources and Safety Engineering, Henan University of Engineering, Zhengzhou 451191,China.(e-mail: weidy103@126.com).

Xin Lv is an undergraduate student at the School of Resources and Safety Engineering, Henan University of Engineering, Zhengzhou 451191, China. (e-mail: 45332589@qq.com).

Zongzhi Wu is a professor at the School of Civil and Resources Engineering, University of Science and Technology Beijing, Beijing 100083, China. (e-mail: wuzongzhi@vip.sina.com).

Zhiyong Shen is a manager at the Sichuan Zhuchuang Safety Technology Co., Chengdu, 610041, China. (e-mail: 343566127@qq.com).

Chen Yu is a manager at the Sichuan Zhuchuang Safety Technology Co., Chengdu, 610041, China. (e-mail: 52208410@qq.com).

Yang Mu is a manager at the Sichuan Zhuchuang Safety Technology Co., Chengdu, 610041, China. (e-mail: 15903739@qq.com).

Tiantian Li is a manager at the Sichuan Zhuchuang Safety Technology Co., Chengdu, 610041, China. (e-mail: 461309933@qq.com).

concentration in each zone. Zou et al.[22,23] analyzed dust concentration measurements in different areas of advancing workfaces and found uneven distribution of dust concentrations in different zones. Lin et al.[24,25] also proposed automatic monitoring and efficient control technologies for underground dust and widely applied them in production and construction in mines.

Based on the above studies, it is evident that numerous scholars have conducted extensive and useful research on dust transport. Due to the difference in dust properties, most of the research has focused on mining sites and advancing workfaces, with relatively limited research on dust transport and concentration distribution in high-speed railway construction tunnels. Ventilation and dust removal are commonly used methods in construction tunnels, and the distribution of airflow within these tunnels directly affects dust transport. Therefore, this study focuses on a specific construction tunnel and performs simulation calculations on the airflow and two-phase flow of dust within the tunnel. We aim to reveal the distribution patterns of airflow and dust concentration on the cross-section at breathing height within the tunnel and provide field parameters and theoretical guidance for the construction of increasingly larger-scale tunnel projects.

II. Materials and Methods

A. The physicochemical properties of tunnel dust

Particle size

Tunnel dust particles are mostly irregular in shape, our use of the term particle refers to each particle's "equivalent diameter." Based on the size of dust particles, they can be roughly divided into two categories. The first category is called "fugitive dust," which refers to particles smaller than 10μm. These particles can float in the atmosphere for a long time and are sometimes referred to as suspended dust. The second category is called "fine dust", which includes particles with diameters ranging from 10μm to 40μm. The concentration of 10μm dust particles is an important reference indicator for ambient air quality.

Concentration

Dust concentration refers to the amount of dust contained per unit volume. According to the regulations[26] on occupational disease prevention and control in work-places only certain maximum concentrations are safe (Table I).

TABLE I
Permissible Dust Concentrations in the Workplace

Dust Type	*Free SiO_2 Content/%*	*Time-weighted Average Permissible Concentration (mg/m³)*	
		Total Dust	*Respiratory Dust*
Coal	<10	4	2.5
	10≤~≤50	1	0.7
Silica	50<~≤80	0.7	0.3
	>80	0.5	0.2
Cement	<10	4	1.5

Adhesiveness

The potential for dust particles to adhere to solid surfaces or coalesce with each other is referred to as the adhesiveness of dust[27], and the force required to overcome the adhesion phenomenon acting vertically on the center of gravity of the particles is called the adhesion force. Generally, dust with smaller particle sizes, rougher surfaces, irregular shapes, high moisture content, good wettability, high dust concentration, and high electric charge exhibits increased adhesion force. Therefore, factors such as ambient humidity, dust particle size, shape, and moisture content, etc. can influence the adhesiveness of dust.

Wettability

The wettability of dust refers to the ease with which dust particles can adhere to or cohere with each other after coming into contact with a liquid. Based on the degree to which dust can be wetted by water, it can be categorized into hydrophobic dust and hydrophilic dust. The wettability of dust is one of the primary considerations in selecting dust removal equipment.

B. Force Analysis of Dust in Tunnels

During the movement of dust in tunnels, various forces such as gravity, buoyancy, drag force, and Brownian motion influence the dust particles. If the dust concentration in the tunnel is low, the main forces acting on the dust are its own gravity and the drag force generated by the fluid. The other forces are relatively small and can be neglected in the calculation process. In this study on the movement of dust generated by tunnel blasting, considering the low volume fraction of dust, only gravity[28] and drag force[29] are taken into account in the calculations.

Gravity

Gravity is the force exerted on dust particles in the air due to their own mass. It can be calculated using the following formula:

$$F_g=\Pi(\rho_p-\rho_a)d_p^3 g/6 \quad (1)$$

where, F_g is the gravitational force acting on the dust particles;

ρ_p,ρ_a are dust concentration and gas concentration, respectively, kg/m^3;

g is acceleration due to gravity, 9.81m/s^2;

d_p is dust diameter, mm.

Drag force

Drag force is the force exerted by a fluid on a solid object that is moving relative to the fluid. This force acts in the opposite direction to the motion of the solid object and represents the resistance to relative motion. The drag force experienced by dust particles moving in the air can be expressed as:

$$F=\Pi C_D \rho_g d_p^2 v^2/8 \quad (2)$$

where, C_D is the drag coefficient;

ρ_g is the air density, kg/m³;

v is the relative velocity of the dust with respect to the air, m/s.

C. Establishment of a physical tunnel model and meshing

A specific high-speed railway tunnel was chosen as the

primary research object. The tunnel has a height of 8.779m and a width of 13.3m. Due to the complex nature of the actual tunnel conditions, certain components such as motors and pipes have been simplified. For the simulation, it is assumed that the tunnel excavation has progressed up to a distance of 200m. Following safety regulations, the distance between the workface and the exit of the forced ventilation duct was determined to be 40m, and the duct has a radius of 0.7m. The vertical direction of the tunnel is represented by the z-axis, and the horizontal direction is represented by the y-axis. Geometric models and meshing can be seen in Figure 1.

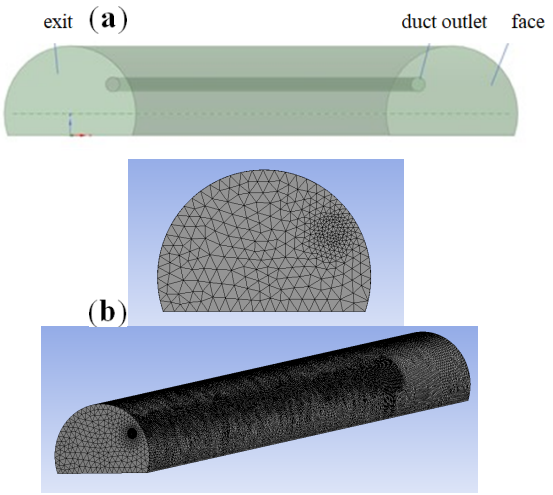

Fig. 1. Schematic of the model (a) Geometric tunnel model (b) Meshing

D. The physicochemical properties of tunnel dust

Basic assumptions

(1) The air inside the tunnel is considered to be an incompressible fluid, and its density is assumed to remain constant.

(2) Fresh air is treated as an ideal gas and is supplied solely through the forced ventilation duct.

(3) The dust generated from blasting is the only instantaneous pollution source; the dust generated from blasting preparation, transportation, and pedestrian movement is neglected.

(4) The dust particles are assumed to be spherical, and the forces resulting from their own rotation are ignored.

Parameterization of continuous phases

TABLE II
UNIAXIAL COMPRESSIVE STRENGTH OF BACKFILL WITH DIFFERENT PARTICLE GRADES

Parameter	*Setting*
Solver	Pressure-based
Time	Steady
Viscous Model	Realizable k-ε
Energy	Off

Based on calculations, it was determined that the fluid flow inside the tunnel exhibits turbulence. The forced ventilation can be considered to be a circular jet, and the tunnel is arch-shaped. Thus, when the airflow reaches the tunnel face, it encounters resistance from the tunnel face and walls. Therefore, the realizable k-ε model was adopted since it can effectively simulate the circular jet in the presence of obstacles from the tunnel face and sidewalls.

Boundary conditions

Based on the actual situation on site, the airflow velocity was set to 13m/s. The inlet of the ventilation duct is defined as a velocity inlet, and the tunnel inlet and outlet were set as outflows.

TABLE III
BOUNDARY CONDITIONS

Parameter	*Setting*
Inlet Boundary Type	Velocity-inlet
Inlet Velocity Magnitude(m/s)	13
Turbulent Intensity	2.77%
Hydraulic Diameter(m)	1.4
Outlet Boundary Type	Outflow
Shear Condition	No slip

Discrete phase parameter settings

The airflow-dust two-phase flow simulation was carried out with the tunnel face as the dust source, and the discrete-phase boundary conditions were set as shown in Table IV.

TABLE IV
DISCRETE PHASE SETTINGS

Type	*Setting*
Solver	Transient
Discrete Phase Model	on
Interaction with Continuous Phase	on
Update DPM Sources Every Flow Iteration	on
Number of Continuous Phase Iterations Per DPM Iteration	10
Unsteady Particle Tracking	on

Dust source and discrete phase boundary conditions

The main component of the dust in the tunnel is SiO_2, with a density of 2320kg/m³. Dust flow rates are typically measured by the mass flow rate, measured in kg/s. Since dust particles are sprayed along the normal direction of the face, this means V_y =-6m/s.

TABLE V
DUST SOURCE SETTINGS

Parameters	*Setting*
Injection Type	Surface
Release From Surface	Face
Diameter Distribution	Rosin-Rammler
Material	SiO_2
Velocity (m/s)	V_y=-6
Total Flow Rate(kg/s)	0.251
Turbulent Dispersion	Random walk model

TABLE VI
DISCRETE PHASE BOUNDARY SETTINGS

Zone	*DPM Condition*	*Shear Condition*
Tunnel Bottom	Trap	No slip
Tunnel Inlet	Escape	No slip
Others	Reflect	No slip

Flow field simulation analysis

After setting the parameters as described in Tables II to III and performing iterative calculations, the corresponding residual curves was obtained as shown in Figure 2. From the figure we can see that convergence was reached at iteration step 504.

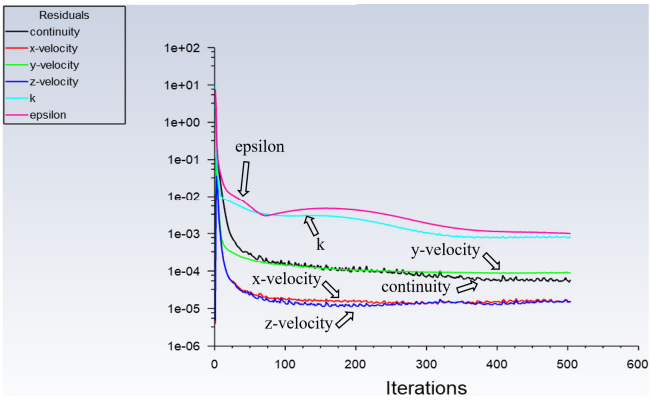

Fig. 2. Residual convergence curve

III. Results and Discussion

A. Flow field distribution in the tunnel

Simulation results and analysis of the airflow field

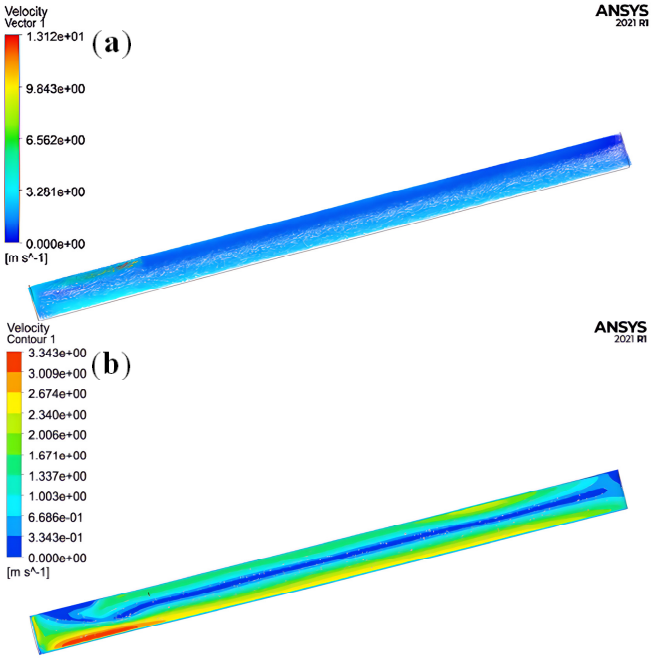

Fig. 3. Variation of airflow field in the tunnel (a)Vector field of airflow (b) Velocity contour plot of airflow in the z=1.5m plane

From Figure 3 we see that the airflow emitted from the outlet of the duct indeed reaches the tunnel face, and the airflow near the face has a velocity of 3m/s, which complies with the requirements stated in the "Technical Regulations for Construction Safety of Railway Tunnel Engineering" (TB10304-2020). Therefore, the distance of 40m from the duct outlet to the face meets the effective range of the jet flow. The airflow distribution from the duct outlet to the face is not uniform. The fresh air from the outlet forms a jet flow, and it interacts with the surrounding air, gradually decreasing the velocity as the airflow section increases. Near the face, there is a backflow in the opposite direction of the jet flow due to the obstructive effect of the face as well. After a certain period of flow, the airflow distribution then stabilizes.

Due to the high airflow velocity at the outlet of the duct, the presence of backflow with velocities opposite to the jet flow can lead to the formation of vortices, which are not conducive to dust removal. In addition, there is a significant gradient difference in the airflow between the duct outlet and the face, and the velocity near the face is approximately 3m/s. Additionally, since the duct is located near the wall, the airflow towards the face generates noticeable wall-attached jet flow. After reflecting off the face, the maximum velocity in the backflow region can reach 3.343m/s.

Simulation results and analysis of dust transport

After the convergence of the airflow field in the tunnel, the discrete phase model was activated with the settings provided in Tables IV to VI. Due to larger dust particles settle and are captured near the tunnel bottom due to gravity. Considering the breathing height of workers, the dust concentration on the z=1.5m in the tunnel was selected as shown in Figure 4.

After blasting, the movement of dust follows the airflow in the tunnel. The dust concentration exhibits a cloud-like distribution with higher concentrations near the wall and lower concentrations in the surrounding areas. The maximum concentration reach 1.33×10^{-2}kg/m³, and the surrounding concentrations are approximately 5×10^{-3}kg/m³. 10s after blasting the dust moves along the wall towards the entrance due to the influence of the backflow, and the maximum dust concentration at breathing height then gradually decreases to 3.641×10^{-3}kg/m³. At 60s, after passing through the duct outlet, the airflow becomes relatively stable, with a maximum velocity of around 2m/s. The central concentration on the bottom decreases to 4.266×10^{-4}kg/m³, and the outer concentrations exceed 2×10^{-4}kg/m³. Next, from 60s to 150s, dust particles begin to detach from the vortices and move towards the entrance with the airflow as a result of the jet and backflow vortices. However, due to gravity, the dust concentration on the breathing height cross-section continues to decrease to 4.959×10^{-5}kg/m³. Finally, after 1800s, the concentration is below the limit of 2mg/m³ specified in the regulations. At this stage, it is considered safe to proceed with construction activities.

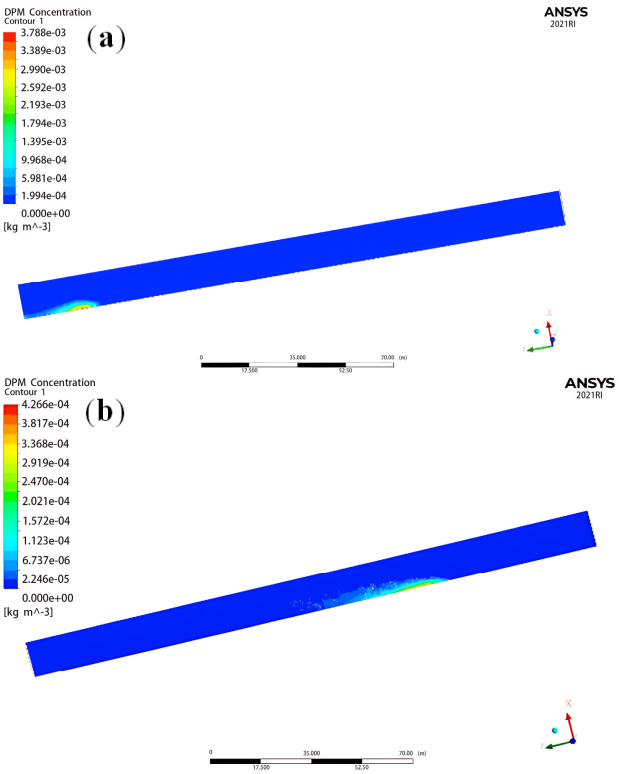

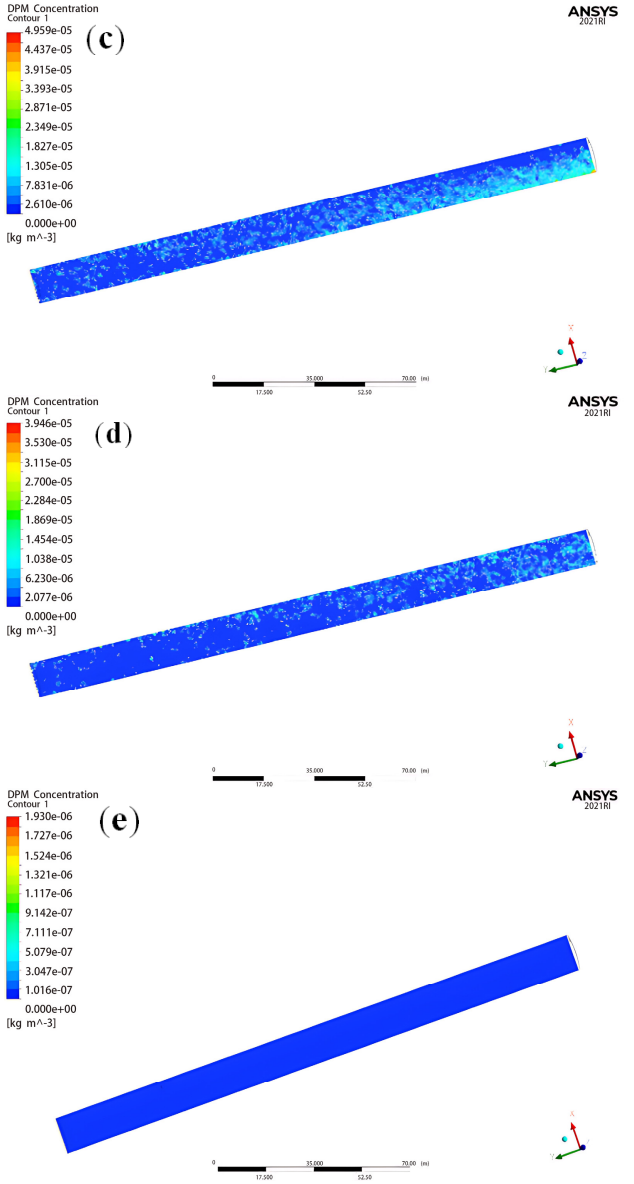

Fig. 4. Dust concentration distribution at different moments (a) 10s (b) 60s (c) 150s (d) 300s (e) 1800s

B. The impact of airflow velocity at the duct outlet on dust transport patterns

Combined with the above simulation results, with 40m of distance from the duct outlet to the face, the airflow velocities of the duct outlet were 13m/s, 16m/s, and 18m/s, respectively.

Distribution of airflow at different outlet airflow velocities

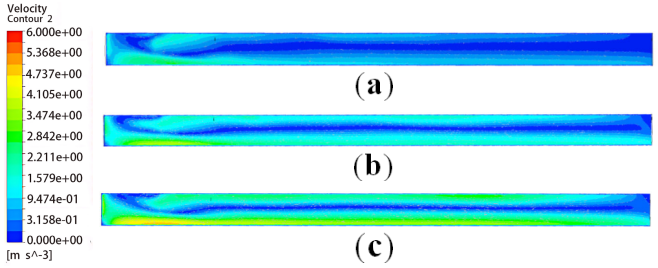

Fig. 5. Velocity distribution with different outlet airflow velocities (a) 13m/s (b) 16m/s (c) 18m/s

The velocity distribution clouds at z=1.5m are shown in Figure 5. When the outlet airflow velocity increases from 13m/s to 18m/s, the airflow distribution near the face remains largely unchanged, the airflow velocity near the face gradually increases from 3m/s to 4m/s. Therefore, increasing the outlet airflow velocity can increase the air intake and improve dust removal efficiency, but it does not have a significant impact on improving the airflow field inside the tunnel.

Dust concentration distribution at different outlet airflow velocities

The variation in dust concentration with different outlet airflow velocities at z=1.5m is shown in Figure 6. With the increase in outlet airflow velocity, the dust migration direction remains consistent, and when the outlet airflow velocity is 18m/s, the dust distribution range is the widest. Moreover, as the outlet airflow velocity increases, the maximum dust concentration gradually decreases. Higher airflow velocities result in greater dust migration distances.

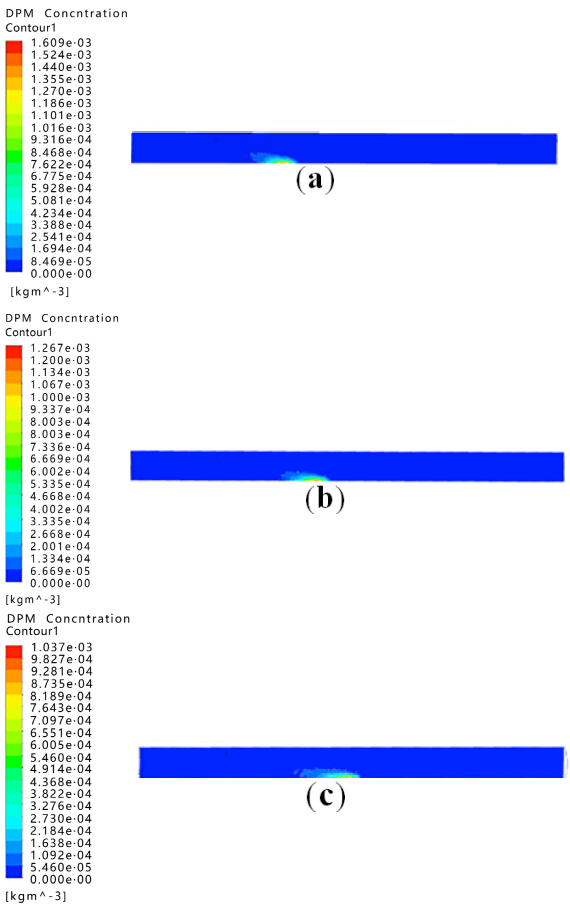

Fig. 6. Dust concentration with different outlet airflow velocities at 30s (a) 13m/s (b) 16m/s (c) 18m/s

Next, from Figure 7 we see that within 100s, some dust particles are transported towards the tunnel entrance by the airflow. For the cases with an outlet velocity of 16m/s and 18m/s, the dust particles have already reached the entrance after 100s of ventilation. Additionally, higher outlet velocities result in a wider dispersion range of the dust particles. In the case of an outlet velocity of 13m/s, the maximum dust concentration is 2.451×10^{-4}kg/m³. This is

because at an outlet velocity of 13m/s, the dust particles have not yet reached the entrance. However, at outlet velocities of 16m/s and 18m/s, higher outlet velocities result in a greater amount of dust particles being expelled from the tunnel.

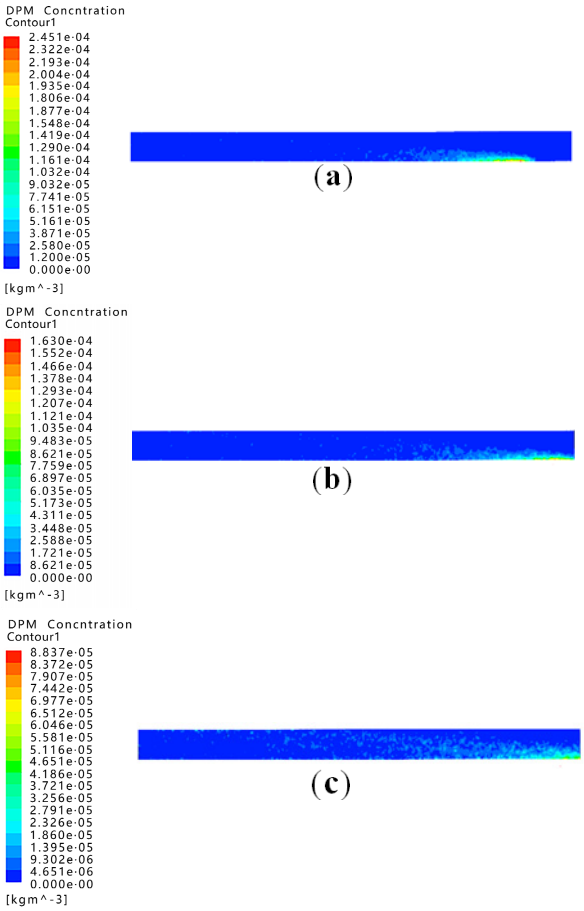

Fig. 7. Dust concentration with different outlet airflow velocities at 100s (a) 13m/s (b) 16m/s (c) 18m/s

Figure 8 shows that at 300s of ventilation, the dust has migrated to the entrance and gradually dispersed throughout the cross-section. The maximum dust concentration is 3.946×10^{-5}kg/m³. This can be attributed to the relatively stable airflow distribution near the entrance and the lower airflow velocity, which allows gravity to have a greater impact in capturing dust particles on the bottom. Moreover, compared to the outlet velocity of 13m/s, when the outlet velocities are 16m/s and 18m/s, the dust primarily accumulates in the latter half of the tunnel. As the outlet velocity increases, however, the maximum dust concentration decreases, with reductions of 6×10^{-6}kg/m³ and 1.4×10^{-5}kg/m³, respectively.

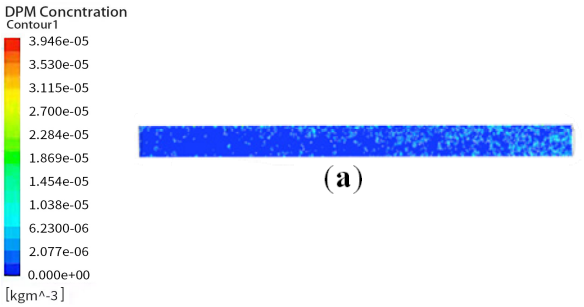

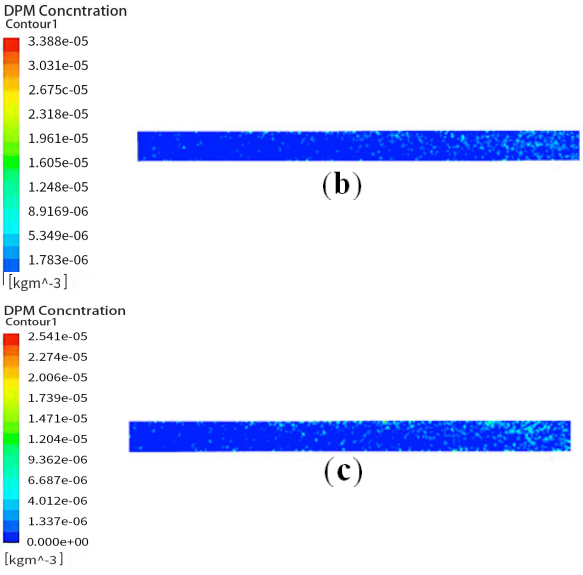

Fig. 8. Dust concentration with different outlet airflow velocities at 300s (a) 13m/s (b) 16m/s (c) 18m/s

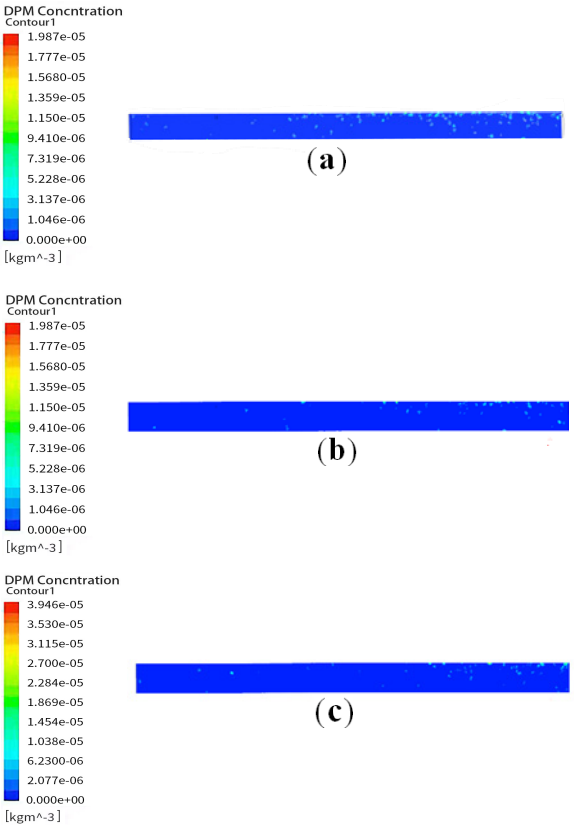

Fig. 9. Dust concentration with different outlet airflow velocities at 1,000s (a) 13m/s (b) 16m/s (c) 18m/s

From Figure 9 we can see that after 1000s of ventilation, the dust has been predominantly discharged on the opposite side of the tunnel from the duct and is concentrated near the installed duct. This is because the respirable dust is less affected by gravity and has difficulty settling, posing a significant health risk to workers. The higher the airflow velocity, the faster the dust is expelled. Therefore, the maximum concentration on the cross-section is lower with higher outlet airflow velocity. Specifically, when the outlet airflow velocity is 18m/s, the maximum dust concentration on the breathing height cross-section is 1.639×10^{-5}kg/m^3.

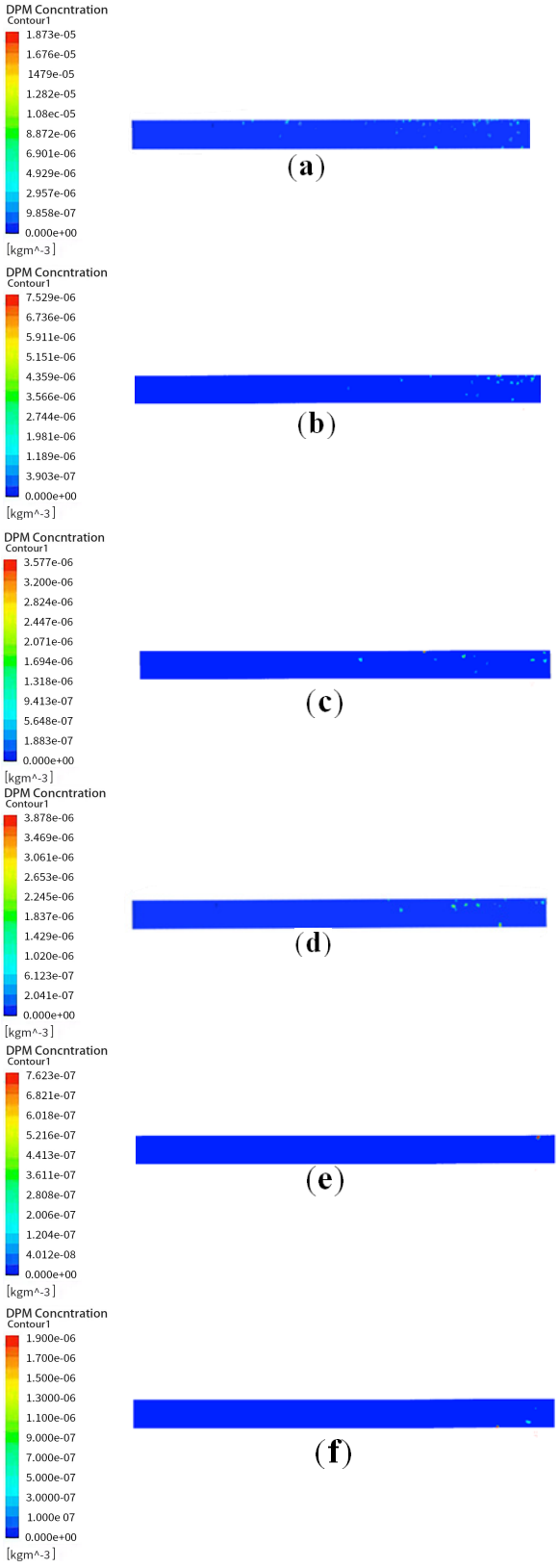

Fig. 10. Dust concentration with different outlet airflow velocities (a) 13m/s, t=1400s (b) 16m/s, t=1,400s (c) 18m/s, t=1400s (d) 13m/s, t=1700s (e) 16m/s, t=1700s (f) 18m/s, t=1700s

Figure 10 shows that the dust concentration in the tunnel decreases continuously from 1400s to 1700s of ventilation. By 1700s, when the airflow velocity is 16m/s or 18m/s, the dust has been largely expelled and is below 2mg/m³, indicating that it is safe to proceed with construction activities. The dust removal efficiency in the tunnel increases with the outlet airflow velocity, with the optimal dust removal efficiency observed at an airflow velocity of 16m/s.

C. The influence of the distance between the wind tunnel outlet and the control surface on the dust migration pattern

To investigate the effect of the distance from the duct outlet to the face on the dust concentration distribution, simulations were performed with different distances between the duct outlet and the face. The outlet airflow velocity was set to 16m/s, and the distances considered were 20m, 30m, and 40m.

Distribution of velocity at different distances

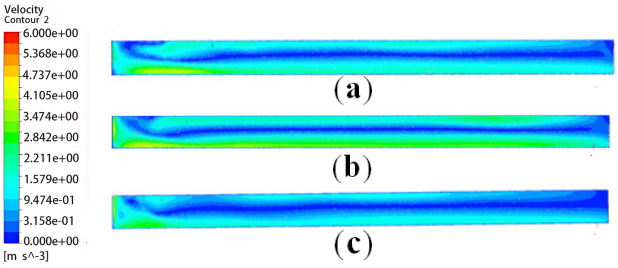

Fig. 11. Velocity distribution at z=1.5m with different distances between the duct outlet and the face (a) 40m (b) 30m (c) 20m

The velocity distribution at z=1.5m are shown in Figure 11. It is evident that the airflow velocity near the face increases as the distance between the duct outlet and the face decreases. The airflow is ejected from the duct outlet and moves along one side of the tunnel towards the face. Upon reaching the face and colliding with the wall, the airflow forms a backflow in the opposite direction of the inlet, and the closer the duct outlet is to the face, the larger the extent of the backflow. When the duct outlet is 20m away from the face, the airflow velocity near the face reaches approximately 5m/s, which is relatively high. Although it complies with the regulation's requirement of 0.15m/s, high airflow velocity increases secondary dust. The backflow is easily influenced by the inlet airflow, resulting in vortex formation between the inlet and backflows, and such vortices are mainly present on the left side of the tunnel and near the face. They tend to trap dust particles and create swirling motions, again hindering dust removal.

Dust concentration distribution at different distances

Figure 12 show that the duct outlet located near one side of the wall injects fresh air into the tunnel. Due to the influence of the airflow, there is almost no dust distribution on the side where the duct is installed in the tunnel. The dust instead mainly moves along the other side of the tunnel with the airflow towards the entrance. Furthermore, as the distance between the duct outlet and the face decreases, the maximum dust concentration gradually increases, reaching a peak concentration of 4.88×10^{-3}kg/m³. This is because the airflow distribution between the duct outlet and the face is unstable, where the airflow near the face causes some dust particles to be carried along with the airflow instead of settling down. When the distance is 20m, the airflow from the duct outlet encounters resistance from the face, forming vortices, and the dust particles circulate within the airflow in eddies, resulting

in a broader distribution of dust concentration compared to 30m and 40m.

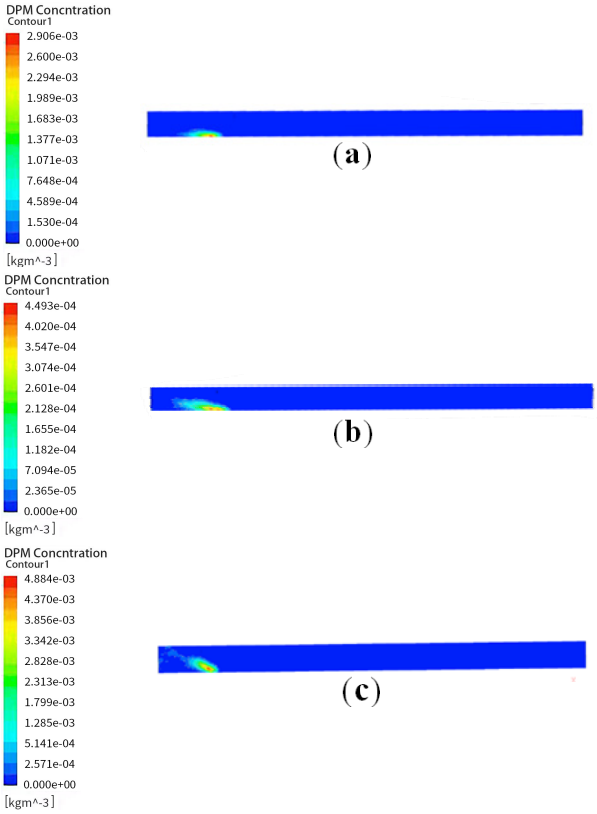

Fig. 12. Dust concentration distribution at different distances at 10s (a) 40m (b) 30m (c) 20m

From Figure 13 we see that after 200s of ventilation, some dust particles are transported towards the entrance along with the airflow. When the distance between the duct outlet and the face is 40m, the dust has dispersed throughout the tunnel. However, when the distance is 30m or 20m, the areas with relatively high dust concentrations are mainly concentrated on one side of the tunnel, and as the distance between the duct outlet and the face decreases, the maximum dust concentration gradually increases. When the duct outlet is 20m away from the face, the maximum dust concentration is 8.865×10^{-5}kg/m^3, and some settled dust particles are resuspended due to the influence of airflow velocity as the airflow moves towards the entrance. After that, the dust particles are discharged from the tunnel with the airflow. As the distance between the duct outlet and the face decreases, the maximum dust concentration increases.

Figure 14 shows that after 500s of ventilation, the dust particles from the distances of 40m and 30m have already moved to the entrance. However, in the tunnel with a distance of 20m, there is still a small amount of dust gathered in irregular dot-like patterns. Additionally, due to the stable airflow velocity near the entrance, dust mostly settles due to gravity, resulting in a noticeable decrease in concentration. And the airflow velocity is higher on the opposite side, causing more dust to be expelled from the tunnel. As a result, the distribution range of dust on the breathing height cross-section is thus significantly reduced. The maximum dust concentration decreases to 2.899×10^{-5}kg/m³.

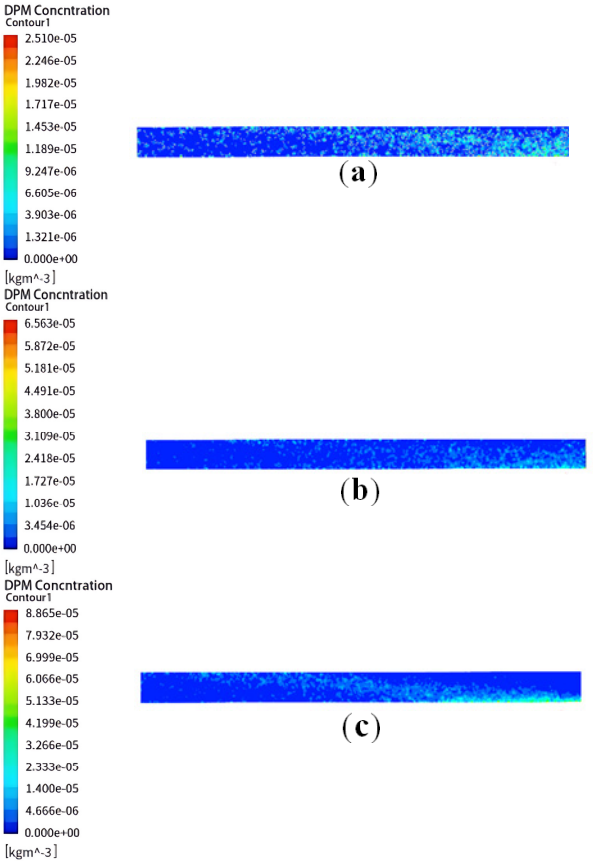

Fig. 13. Dust concentration distribution at different distances at 200s (a) 40m (b) 30m (c) 20m

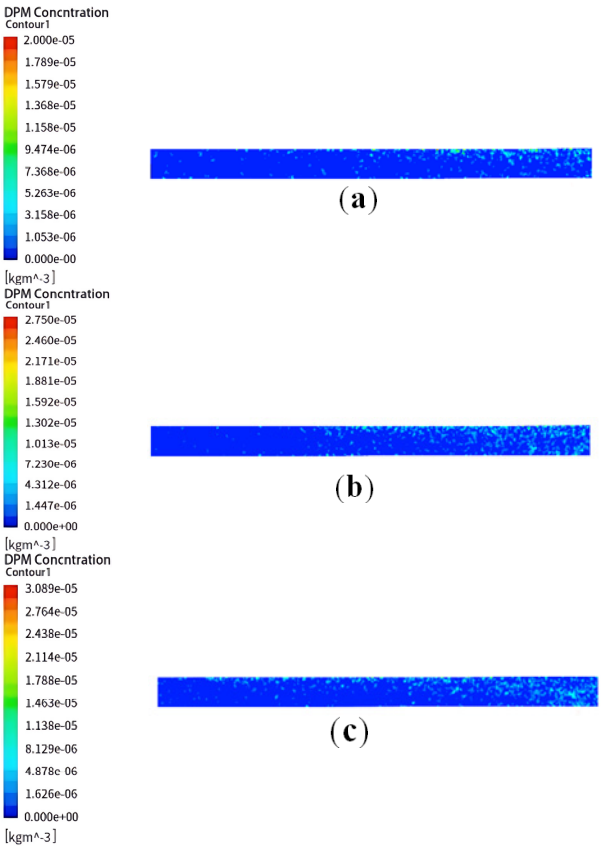

Fig. 14. Dust concentration distribution at different distances at 500s (a) 40m (b) 30m (c) 20m

As can be seen from Figure 15, when the distance between the duct outlet and the face is 40m, after 1700s of ventilation,

the dust particles are effectively expelled from the tunnel. The dust concentration is below the permissible concentration of 2mg/m³ as specified in the regulations. When the distance is 30m, after 1300s of ventilation, the dust particles have been mostly expelled from the tunnel, with only a small amount of dust accumulating at the entrance, but the maximum dust concentration is also below 2mg/m³. When the distance is 20m, after 1600s of ventilation, the dust particles are effectively expelled from the tunnel leaving a concentration of 2mg/m³ and allowing for construction activities to resume.

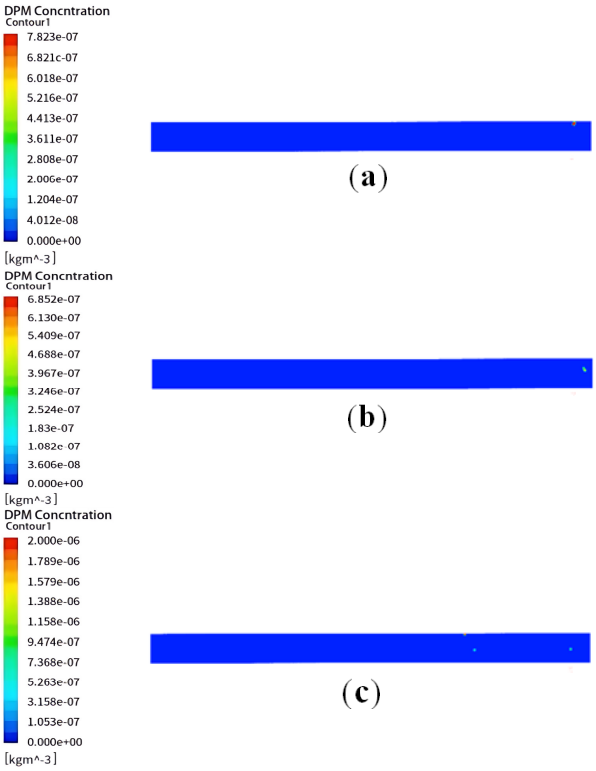

Fig. 15. Variation of dust concentration at different distance between the duct outlet and the face (a) L=40m, t=1700s (b) L=30m, t=1300s (c) L=20m, t=1600s

Reducing the distance between the duct outlet and the face effectively reduces the time required for the tunnel dust to be completely discharged. When the distance between the duct outlet and the face is reduced to 30m, the shortest time for complete dust expulsion is achieved of all distances we tested, with ventilation for 1300s being sufficient. However, further reducing the distance to 20m can lead to the re-entrainment of settled dust due to secondary dust generation and vortex formation, resulting in an increased time required for complete dust expulsion. When the distance is reduced to 20m, the airflow velocity near the face reaches approximately 5m/s. Due to the proximity to the outlet, the inlet airflow is obstructed by the face, resulting in a backflow that hinders dust expulsion and reduces the efficiency of dust removal.

IV. Conclusions

The important conclusions from this study are enumerated below.

(1) When the outlet airflow velocity increases from 13m/s to 16m/s, the airflow velocity near the face increases, causing some dust particles to settle due to gravity, while others move towards the entrance with the airflow, the maximum dust concentration decreases. When the airflow velocity increases to 18m/s, the increased airflow velocity near the face causes some of the settled dust particles to be resuspended, and the maximum concentration increased to 3.462×10^{-3}kg/m³.

(2) After 30s of ventilation, the dust concentration on the breathing height cross-section of the tunnel decreases with an increase in the outlet airflow velocity. Between 30s and 100s of ventilation, the distribution of airflow inside the tunnel is similar, and the maximum concentration decreases with an increase in the outlet airflow velocity. A higher outlet airflow velocity leads to a wider dispersion range of dust.

(3) Between 300s and 1400s of ventilation, some dust particles are captured by the bottom, while others are continuously expelled with the airflow, and the expulsion rate increases with higher airflow velocities. After 1700s of ventilation, when the outlet airflow velocities are 16m/s and 18m/s, the dust is effectively expelled from the tunnel, and the dust concentration on the breathing height cross-section meets the safety standards.

Acknowledgments

The authors thank AiMi Academic Services (www.aimieditor.com) for English language editing and review services.

References

[1] F. Yin, S. Mei. Statistical bulletin on the development of the transport industry in 2022. *J. Waterw. Harbor* 2023, vol. 44, no. 6, pp. 1002, 1006.

[2] J. Gong, G. Tang, W. Wang, et al. Statistics on China's railroad tunnels by the end of 2021 and Overview of Gaoligong Mountain tunnel design and construction. *Tunnel Constr.* 2022, vol. 42, no. 3, pp. 508–517.

[3] F. Anlimah, V. Gopaldasani, C. MacPhail, et al. A systematic review of the effectiveness of dust control measures adopted to reduce workplace exposure. *Environ. Sci. Pollut. Res.* 2023, vol. 30, no. 19, pp. 1–22.

[4] B. Men, Q. Ma. Harm of tunnel dust particles and control measures. *Transp. Energy Conser. Environ. Prot.* 2021, vol.17, no. 1, pp. 144–147.

[5] Z. Bai, Y. Yu, Y. Zhang, et al. Experimental study on the influence of sealing and ventilation on the fire characteristics near the wall of utility tunnel. *IAENG Int. J. Appl. Math.* 2024, vol.54, no. 5, pp. 866–887.

[6] K. Ren, A. Jiang, X. Guo, et al. Research on optimization design of tunnel blasting scheme adjacent to buildings. *Appl. Sci.* 2023, vol.13, no. 20, pp. 11509.

[7] L. Kyle, J. Patts, H. Emily, et al. Evaluation of engineering controls at bagging operations to reduce exposures to respirable crystalline silica dust. *Min. Metall. Explor.* 2020, vol.37, no. 1.

[8] T. Irgibayev, I. Lugin, L. Kiyanitsa. Justification of an energy-efficient air purification system in subways based on air dust content studies. *Build.* 2023, vol.13, no. 11, pp. 2771.

[9] T. Feroze, B. Genc. Evaluation of line brattice length in an empty heading to improve air flow rate at the face using CFD. *Int. J.Min. Sci. Technol.* 2017, vol.27, no. 2, pp. 253–259.

[10] M. Chung. Study on the two-phase critical flow through a small bottom break in apressurized horizontal pipe. *J. Sound Vib.* 2018, vol.313, no. 1, pp. 7–15.

[11] L. Wang, C. Li, C. Li. A short-term wind speed prediction method based on the DGA-BP neural network. *IAENG Int. J. Comp. Sci.* 2024, vol.51, no. 5, pp. 496–505.

[12] Y. Cheng, H. Tao, X. Lu, et al. Prediction method of axial compression capacity of CCFST columns based on deep learning," *IAENG Int. J. Comp. Sci.* 2024, vol.51, no.3, pp. 243–251.

[13] I. Tuleukhan, L. Vladimirovich, K. Lavrentiy. Justification of an energy-efficient air purification system in subways based on air dust content studies. *Build.* 2023, vol.13, no. 11, pp. 2771.

[14] S. Mikhail, A. Isaevich, S. Zhikharev. The analysis of potash salt dust deposition in roadways. *J. Min. Sci.* 2021, vol.57, no. 2, pp. 341–353.

[15] K. Koshiro, H. Hisashi, T. Mitsutoshi. Simulation of chronological change in dust concentration during tunnel construction by unsteady CFD analysis. *J. Jpn. Soc. Civ. Eng.* 2022, vol.78, no. 1, pp. 13–25.
[16] T. Du, W. Nie, D. Chen, et al. CFD modeling of coal dust migration in an 8.8-meter-high fully mechanized mining face. *Energy* 2020, vol.212, no. 4, pp. 118616.
[17] C. Guo, W. Nie, C. Xu, et al. A study of the spray atomization and suppression of tunnel dust pollution based on a CFD-based simulation. *J. Cleaner Prod.* 2020, vol.276, no. 2, pp. 276–278.
[18] P. Cai, W. Nie. Study on the air curtain dust control technology with a dust purifying fan for fully mechanized mining face. *Powder Technol.* 2020, vol.374, pp. 156–167.
[19] F. Oriol, M. Teresa, Q. Xavier, et al. Origin and speciation of major and trace PM elements in the Barcelona subway system. *Transp. Res. Part D Transp. Environ.* 2019, vol.72, no. 1506–1516, pp. 17–35.
[20] W. Reed, S. Klima, A. Mazzella, et al. A second case study of field test results for comparison of roof bolter dry collection system with wet collection system. *Min. Metall. Explor.* 2022, vol.39, no. 2.
[21] F. Hasheminasab, R. Bagherpour, S. Aminossadati. Numerical simulation of methane distribution in development zones of underground coal mines equipped with auxiliary ventilation. *Tunnelling Underground Space Technol.* 2019, vol.89, no. 1, pp. 68–77.
[22] C. Zou. Study on optimization and application of high-pressure spray parameters. *Min. Saf. Environ. Prot.* 2016, vol.43, no. 6, pp. 9–12.
[23] A. Isaevich, M. Semin, L. Levin, et al. Study on the dust content in dead-end drifts in the Potash mines for various ventilation modes. *Sustainability* 2022, vol.14, no. 5, pp. 3030.
[24] X. Lin, Z. Liu, N. Geng, et al. Optimization and application of water injection process in gas-bearing coal seam. *Processes* 2023, vol.11, no. 10, pp. 3003.
[25] Y. Voroshilov, D. Trubitsyna. Dust deposition intensity method and control system development in order to increase the underground coal mine openings dust explosion safety. *Ind. Saf.* 2017. no. 4. pp. 28–41.
[26] State Administration of Work Safety. Regulations on the prevention and control of occupational disease hazards in workplaces. 2015.
[27] J. Liu, H. Zhang, Y. Zhou, et al. Design and optimization of a novel dust collection device for underground dry drilling based on numerical simulation and field testing. *Processes* 2023, vol.11, no. 10, pp. 2942.
[28] L. Jin, J. Liu, Q. Lin, et al. Review on the research and application of water spray dust-reduction technology in mines. *Met. Mine* 2023, no. 7, pp. 2–17.
[29] H. Yu, I. Zahidi. Environmental hazards posed by mine dust, and monitoring method of mine dust pollution using remote sensing technologies: An overview. *Sci. Total Environ.* 2022, vol.864, no. 3, pp. 161135.